



Dynamic coupling of photoacclimation and photoinhibition in a model of microalgae growth

Andreas Nikolaou, Philipp Hartmann, Antoine Sciandra, Benoît Chachuat,
Olivier Bernard

► To cite this version:

Andreas Nikolaou, Philipp Hartmann, Antoine Sciandra, Benoît Chachuat, Olivier Bernard. Dynamic coupling of photoacclimation and photoinhibition in a model of microalgae growth. *Journal of Theoretical Biology*, 2016, 390, pp.61 - 72. 10.1016/j.jtbi.2015.11.004 . hal-01247049

HAL Id: hal-01247049

<https://inria.hal.science/hal-01247049>

Submitted on 15 Apr 2021

HAL is a multi-disciplinary open access archive for the deposit and dissemination of scientific research documents, whether they are published or not. The documents may come from teaching and research institutions in France or abroad, or from public or private research centers.

L'archive ouverte pluridisciplinaire **HAL**, est destinée au dépôt et à la diffusion de documents scientifiques de niveau recherche, publiés ou non, émanant des établissements d'enseignement et de recherche français ou étrangers, des laboratoires publics ou privés.

Dynamic Coupling of Photoacclimation and Photoinhibition in a Model of Microalgae Growth

Andreas Nikolaou^{a,b,*}, Philipp Hartmann^{b,c,*}, Antoine Sciandra^b, Benoît Chachuat^{a,**},
Olivier Bernard^{b,c}

^a*Centre for Process Systems Engineering (CPSE), Department of Chemical Engineering, Imperial College
London, London SW7 2AZ, UK*

^b*Sorbonne Universités, UPMC Univ Paris 06, and CNRS, UMR 7093, LOV, Observatoire Océanologique,
F-06230, Villefranche sur Mer, France*

^c*BIOCORE-INRIA, BP93, 06902 Sophia-Antipolis Cedex, France*

Abstract

The development of mathematical models that can predict photosynthetic productivity of microalgae under transient conditions is crucial for enhancing large-scale industrial culturing systems. Particularly important in outdoor culture systems, where the light irradiance varies greatly, are the processes of photoinhibition and photoacclimation, which can affect photoproduction significantly. The former is caused by an excess of light and occurs on a fast time scale of minutes, whereas the latter results from the adjustment of the light harvesting capacity to the incoming irradiance and takes place on a slow time scale of days. In this paper, we develop a dynamic model of microalgae growth that simultaneously accounts for the processes of photoinhibition and photoacclimation, thereby spanning multiple time scales. The properties of the model are analyzed in connection to PI-response curves, under a quasi steady-state assumption for the slow processes and by neglecting the fast dynamics. For validation purposes, the model is calibrated and compared against multiple experimental data sets from the literature for several species. The results show that the model can describe the difference in photosynthetic unit acclimation strategies between *D. tertiolecta* (n-strategy) and *S. costatum* (s-strategy).

Keywords: microalgae, photosynthesis modeling, Droop model, Han model, acclimation strategy, PI curves

*Equal contributors

**Corresponding author

1. Introduction

Microalgae are often considered a promising alternative for production of renewable energy [35]. Claimed advantages of this approach are a higher photosynthetic yield compared to field crops, a reduction in fresh water consumption, and independence to agriculturally usable land [36]. These advantages could lead to large-scale production of algal biomass that is not in direct competition with food production. Moreover, microalgae culture systems can be coupled with wastewater treatment technologies [29], can produce high added-value products such as cosmetics, pharmaceuticals and nutraceuticals [6], and can even contribute to CO₂ mitigation due to their inherent ability to fix carbon during photosynthesis [32]. Nonetheless, numerous problems need to be overcome on the path to a sustainable large-scale biofuel production. Optimizing the entire production chain in order to reduce the production costs as well as the environmental impact presents many challenges, and among them improving the algal biomass production efficiency has top priority. As well as developing a better understanding of the key mechanisms underlying photosynthesis, the development of more accurate mathematical models combining mass-conservation principle and phenomenological knowledge holds much promise in this context [5].

Two key processes are involved in the way light conditions affect the photosynthetic yield. *Photoinhibition* causes a loss of photosynthetic yield due to an excess of photons, which damage some of the key proteins in the photosynthetic apparatus. *Photoacclimation*, the process by which microalgae adjust their pigment content and composition to light intensity, alters the rate of photosynthetic production. These two processes act on different time scales: photoinhibition occurs on a time scale of minutes, whereas photoacclimation acts on a time scale of days. In order to achieve optimal microalgae productivity, understanding the processes of nutrient assimilation, photoinhibition and photoacclimation, together with their interactions, is thus paramount. A number of mathematical models are available that account for photoacclimation and nitrogen limitation at the slow time scale [15, 2, 16], yet they neglect the dynamics of photoinhibition. Conversely, models describing photoinhibition in the fast time scale have also been proposed [10, 17], but they do not account for photoacclimation.

The model by Camacho and coworkers [14], inspired from [37, 38], describes both photoinhibition and photoacclimation in nitrogen replete conditions. In contrast, the main objective of this paper is to develop a dynamic model of microalgae growth that couples photoinhibition and photoacclimation under nitrogen limitation. With regards to carbon and nitrogen uptake, our model builds upon two well established models, which have been validated experimentally and whose mathematical properties are well established. Nutrient assimilation is described by the well-accepted and validated Droop model [8]. Photoinhibition is described by the model proposed by Han [17], originating in the work of Eilers and Peeters [10] who first introduced the concept of photosynthetic factories—also known as photosynthetic units. A related, yet simpler, coupling between a photoinhibition model and the Droop model has been studied by Hartmann et al. [19]. An extension of this coupling incorporating photoacclimation processes constitutes the main novelty of the developed model. Specifically, we propose a modification of the photosynthesis rate and pigment synthesis rate expressions to account for photoacclimation effects, and we express both the effective cross-section and the number of photosynthetic units—which are parameters in the Han model—as functions of the chlorophyll content by means of empirical relations [12]. This approach leads to a simple expression for the photosynthesis rate, which is readily amenable to mathematical analysis under a quasi-steady-state approximation. This structure also makes the model easier to calibrate, and we illustrate its prediction capabilities for three different species based on literature data.

The remainder of this paper is organized as follows. Existing models of slow and fast processes, including nutrient limited growth, photoacclimation and photoinhibition, are first reviewed in Sect. 2. The dynamic model coupling these processes is described in Sect. 3, and the properties of the resulting PI-response model are analyzed. A calibration of the coupled model against several experimental data sets from the literature is presented in Sect. 4, followed by a discussion in Sect. 5. Finally, Sect. 6 concludes the paper and draws future research directions.

2. Modeling of Slow and Fast Processes in Microalgae

2.1. Nutrient-Limited Growth – The Droop Model

Droop [7] first observed that microalgae keep growing for some time after nutrients have been depleted. Monod kinetics are unable to model this behavior and therefore are not suitable for predicting microalgae growth under nutrient limitation. A better way to represent nutrient-limited growth is by separating the nutrient uptake rate, denoted by ρ hereafter, from the growth rate, denoted by μ . This idea was followed by Droop [7, 8] in relating the growth rate to the internal elemental nutrient quota. Since its introduction, the Droop model has been widely studied [22, 3, 34] and thoroughly validated [8, 28, 4, 34]. A key feature of our model in Sect. 3 is to build upon this model in order to inherit its structural properties.

In a continuous and homogeneous microalgae culture, the mass-balance equations for the nutrient (inorganic nitrogen) concentration s [$\text{g}_\text{N} \text{m}^{-3}$] in the bulk phase, the biomass concentration x [$\text{g}_\text{C} \text{m}^{-3}$], and the carbon-specific nitrogen quota q [$\text{g}_\text{N} \text{g}_\text{C}^{-1}$] of the cells are given by

$$\begin{aligned}\dot{s} &= D s_{\text{in}} - \rho(s, q) x - D s \\ \dot{x} &= \mu(q, \cdot) x - D x - R x \\ \dot{q} &= \rho(s, q) - \mu(q, \cdot) q,\end{aligned}\tag{1}$$

with D [s^{-1}] and R [s^{-1}] denoting the dilution rate and the endogenous respiration rate, respectively; and s_{in} [$\text{g}_\text{N} \text{m}^{-3}$], the nutrient concentration in the feed.

Recently, an extension of the Droop model has been proposed by Bernard [2] accounting for the effect of light conditions on the growth rate μ in the form

$$\mu(q, \cdot) = \bar{\mu} \left(1 - \frac{Q_0}{q} \right) \phi(\cdot),\tag{2}$$

where $\bar{\mu}$ [s^{-1}] stands for the maximal growth rate, i.e., the growth rate reached under non-limiting conditions; Q_0 [$\text{g}_\text{N} \text{g}_\text{C}^{-1}$], the minimal cell quota, so that $\mu(Q_0, \cdot) = 0$ and $q \geq Q_0$; and, $\phi(\cdot)$ is a saturation function. In particular, an expression of $\phi(\cdot)$ will be developed in Sect. 3 that accounts for the state of the photosynthetic units (PSUs).

The nutrient uptake rate ρ , on the other hand, can be expressed as [16]

$$\rho(s, q) = \bar{\rho} \frac{s}{s + k_s} \left(1 - \frac{q}{Q_l} \right), \quad (3)$$

where $\bar{\rho}$ [$\text{g}_\text{N} \text{g}_\text{C}^{-1} \text{s}^{-1}$] stands for the maximal nutrient uptake rate; k_s [$\text{g}_\text{N} \text{m}^{-3}$], the half-saturation constant for substrate uptake; and Q_l [$\text{g}_\text{N} \text{g}_\text{C}^{-1}$], the limit quota for the nitrogen uptake, so that $\rho(s, Q_l) = 0$ and $q \leq Q_l$, with equality corresponding to nutrient-replete conditions.

2.2. Pigment Content

Photoacclimation is the mechanism by which both the chlorophyll content and the pigment composition change in response to variations in the light irradiance. Such changes take place on a time scale of days, and it has been suggested that microalgae use photoacclimation as a means to optimize their growth at low irradiance as well as to minimize damage at high irradiance [12].

One way to describe photoacclimation is by accounting for the change in the chlorophyll content over time. Following Bernard [2], the chlorophyll concentration, c [$\text{g}_\text{chl} \text{m}^{-3}$], is assumed to be proportional to cellular protein concentration as a first approximation, which is itself represented by the particulate nitrogen concentration $x q$:

$$c = \psi(I_g) x q, \quad (4)$$

where I_g [$\mu\text{E} \text{m}^{-2} \text{s}^{-1}$] represents the light irradiance at which the cells are acclimated, also called *growth irradiance*. Introducing the carbon-specific chlorophyll quota $\theta := c/x$ [$\text{g}_\text{chl} \text{g}_\text{C}^{-1}$], the foregoing relation can be rewritten in the form

$$\theta = \psi(I_g) q. \quad (5)$$

Here, we choose to express $\psi(\cdot)$ in the form of the hyperbolic function

$$\psi(I_g) = \bar{\psi} \frac{k_I}{I_g + k_I}, \quad (6)$$

with parameters $\bar{\psi}$ [$\text{g}_\text{chl} \text{g}_\text{N}^{-1}$] and k_I [$\mu\text{E} \text{m}^{-2} \text{s}^{-1}$]. Moreover, the dynamic evolution of I_g is

related to the current light irradiance I by the following equation

$$\dot{I}_g = \delta \mu(q, \cdot) (I - I_g), \quad (7)$$

thereby assuming that the acclimation rate is proportional to the irradiance difference $(I - I_g)$ as well as to the current growth rate $\mu(\cdot)$, with the constant proportionality coefficient $\delta [-]$. On the whole, a change in the current irradiance I affects I_g via (7), modifying the chlorophyll quota θ via (5) in turn.

2.3. Photosynthetic Production and Photoinhibition – The Han Model

The Han model [17], which is inspired by the model of Eilers and Peeters [9], describes the effect of light irradiance on microalgae growth. This model considers the damage of key proteins in PSUs to be the main contribution to photoinhibition. Particularly appealing in the Han model is the description of complex photosynthetic processes in terms of three possible states of the PSUs only, namely: open, A ; closed, B ; and, inhibited, C .

The equations giving the rates of change in the fractions of open, closed and inhibited PSUs are in order:

$$\begin{aligned} \dot{A} &= -I \sigma A + \frac{B}{\tau} \\ \dot{B} &= I \sigma A - \frac{B}{\tau} + k_r C - k_d \sigma I B \\ \dot{C} &= -k_r C + k_d \sigma I B, \end{aligned} \quad (8)$$

with initial conditions such that $A(0) + B(0) + C(0) = 1$. A number of remarks are:

- Photosynthetic production is described by the transition between open state and closed state. Excitation is assumed to occur at a rate of σI , with $\sigma [\text{m}^2 \mu\text{E}^{-1}]$ the effective cross-section of the PSUs, whereas deexcitation is assumed to occur at a rate of $\frac{1}{\tau}$, with $\tau [\text{s}]$ the turnover time of the electron transport chain.
- Photoinhibition occurring at high light irradiance corresponds to the transition from closed state to inhibited state. This process is assumed to occur at a rate of $k_d \sigma I$, with $k_d [-]$ a damage constant. The reverse transition from inhibited state to closed

state accounts for the repair of damaged PSUs by enzymatic processes in the cell, a mechanism that is assumed to occur at a constant rate k_r [s⁻¹].

The Han model provides the second brick in our model in Sect. 3, also with the objective of keeping its structural properties. In particular, an interesting property of the Han model is that the fractions of open, closed and inhibited states can be computed analytically from (8) as a function of the irradiance I at steady state. For instance, the steady-state expression A^∞ for the open state A is given by:

$$A^\infty(I) = \frac{1}{1 + \tau \sigma I + K \tau \sigma^2 I^2}, \quad (9)$$

with $K := k_d/k_r$.

3. Multi-Scale Model of Microalgae Growth Coupled with Photoinhibition and Photoacclimation

The proposed model couples three dynamic processes, namely (i) the PSU dynamics, (ii) the dynamics of intracellular nitrogen content, and (iii) the dynamics of chlorophyll content. These processes span four different timescales ranging from milliseconds for the open-closed dynamics of the PSUs up to several days for the dynamics of intracellular nitrogen quota q .

3.1. Coupling Between Growth, Photoinhibition and Photoacclimation

Our model builds upon the Droop-Han model of Hartmann et al. [19] and incorporates photoacclimation processes via the dynamics of the chlorophyll quota θ introduced in Sect. 2.2. More specifically, we account for two possible ways that the term $\phi(\cdot)$ in (2) can depend on θ . The first effect is a direct linear dependency of photosynthesis efficiency on the chlorophyll content, which is in agreement with the work of Faugeras et al. [13]. Since the probability of a photon encountering an open state is proportional to AI , a second, indirect effect is via the dependence of the dynamics of A on θ . This latter dependency results from the fact that the parameter σ introduced in the Han model (8) can itself depend on the current acclimation state. Indeed, Falkowski and Raven [12] describe photoacclimation

as a process that can follow either one of two strategies: the *n-strategy* corresponds to a change in the density (per biomass unit) of PSUs, denoted by N subsequently; the *s-strategy* corresponds to a change in the size of the PSUs, and is thus directly related to the effective cross-section σ . In practice, chlorophyll is thus used either to build new PSUs or to increase the size of the antenna in existing PSUs. These two acclimation strategies run concurrently, and both can be described by defining $N(\cdot)$ and $\sigma(\cdot)$ as functions of the chlorophyll quota θ . Such relationships are further investigated in Sect. 3.3.

Based on the above, the growth rate μ can be modeled as:

$$\mu(q, \theta, I) = \bar{\alpha} \left(1 - \frac{Q_0}{q}\right) \theta A(I, \theta) I,$$

where $\bar{\alpha}$ is a constant parameter. At this point, we shall introduce the rate of carbon uptake per chlorophyll unit, μ_{chl} [$\text{g}_\text{C} \text{g}_{\text{chl}}^{-1} \text{s}^{-1}$], as

$$\mu_{\text{chl}}(q, \theta, I) = \frac{\mu(q, \cdot)}{\theta} = \bar{\alpha} \left(1 - \frac{Q_0}{q}\right) A(I, \theta) I, \quad (10)$$

which is also known as the chlorophyll-specific photosynthesis rate.

3.2. Structural Analysis of the PI Response

In experiments assessing photosynthetic efficiency of microalgae, the cells are photoacclimated to a given light irradiance I_g for a sufficiently long time and under nutrient replete conditions, before exposing them to various light irradiances I . The instantaneous growth rates obtained under these conditions—ideally via consideration of the carbon fixation rate, but often based on the O_2 production rate too—are measured and yield the so-called PI-response curve when plotted against I .

A common assumption about PI-response curve experiments is that they are fast enough for photoacclimation, substrate internalization and growth to be negligible; that is, time variations in the variables θ , q and x can all be neglected. In contrast, variations in the fractions of open, closed and inhibited states in the Han model can be considered fast in the time scale of PI-response curve experiments, and one can thus assume that the variables A , B and C reach their steady states as in (9), without significantly impairing the PI response

predictions (quasi-steady-state approximation). Under nutrient-replete conditions, these approximations lead to the following simplification of the chlorophyll-specific photosynthesis rate (10):

$$\mu_{\text{chl}}^{\text{PI}}(\theta, I) = \bar{\alpha} \left(1 - \frac{Q_0}{Q_{\text{max}}(\cdot)} \right) \frac{I}{1 + \tau \sigma(\theta) I + K \tau \sigma^2(\theta) I^2}, \quad (11)$$

where $Q_{\text{max}}(\cdot)$ [$\text{g}_\text{N} \text{g}_\text{C}^{-1}$] denotes the maximal value of the nitrogen internal quota q under nutrient replete conditions, a value that typically depends on the growth irradiance I_g [2]. A further reformulation gives

$$\mu_{\text{chl}}^{\text{PI}}(\theta, I) = \alpha(\cdot) \frac{I}{1 + \tau \sigma(\theta) I + K \tau \sigma^2(\theta) I^2}, \quad (12)$$

with $\alpha(\cdot) := \bar{\alpha} \left(1 - \frac{Q_0}{Q_{\text{max}}(\cdot)} \right)$ [$\text{g}_\text{C} \text{g}_\text{chl}^{-1} \mu\text{E}^{-1} \text{m}^2$] denoting the initial slope of the PI response curve, i.e., the rate of change of μ_{chl} with respect to the light irradiance I for a vanishing irradiance.

Many authors concur to say that, for many microalgae species, the initial slope $\alpha(\cdot)$ can be considered to be independent of the value of θ [23]. Nonetheless, we like to note that the constant initial slope assumption is still debated; see, for instance, the paper by Richardson et al. [27], where microalgae acclimation strategies are divided into six different categories based on photosynthesis-irradiance response data. We shall come back to this important point later on in Sect. 5, where it is argued that certain variations in initial slopes may as well be explained by transient effects in the fraction of inhibited PSUs.

In the remainder of this subsection, we investigate structural properties of the PI-response curve under the foregoing assumptions of time-scale separation and constant initial slope. The optimal irradiance value I^\star maximizing $\mu_{\text{chl}}^{\text{PI}}$ can be determined from (12) as

$$I^\star(\theta) := \frac{1}{\sigma(\theta) \sqrt{K \tau}}. \quad (13)$$

In turn, the maximal productivity rate $\mu_{\text{chl}}^{\text{PI}^\star}$ can be expressed in the form

$$\mu_{\text{chl}}^{\text{PI}^\star}(\theta) := \alpha \frac{\sqrt{K \tau}}{\tau + 2\sqrt{K \tau}} I^\star(\theta). \quad (14)$$

The following property follows readily from (14), provided that the Han model parameters τ and K are independent of the acclimation state:

Property 1. *The maximal growth rate $\mu_{\text{chl}}^{\text{PI}\star}$ is proportional to the optimal irradiance I^\star regardless of the pre-acclimated state or the growth irradiance.*

Although a direct consequence of the constant initial slope assumption, this property does not depend on a particular choice of the relationship between $\sigma(\cdot)$ and θ . Moreover, it is readily tested using data from experimental PI curves corresponding to different acclimation states—see Sect. 4.1.

3.3. Quantitative Analysis of the PI Response

In order to make quantitative predictions of the PI-response curve or, more generally, for numerical simulation of the coupled model, relationships for the effective cross-section $\sigma(\cdot)$ and the density of PSUs $N(\cdot)$ in terms of the chlorophyll quota θ must be specified.

We start by noting that $\sigma(\theta)$ and $N(\theta)$ can both be related to the average size of a PSU in terms of chlorophyll content per PSU, denoted by $\Gamma(\theta)$ subsequently. A simple relation for $N(\theta)$ is:

$$\Gamma(\theta) N(\theta) = \theta. \quad (15)$$

On the other hand, the relation between $\sigma(\theta)$ and $\Gamma(\theta)$ or $N(\theta)$ is highly complex. As well as the geometric shape of the photosynthetic antennas, this relation must take into account the packaging effect and the synthesis of other accessory pigments. Here, we choose to use a simple relationship, whereby $\sigma(\cdot)$ is expressed as a power law of Γ :

$$\sigma(\theta) = \sigma_0 \Gamma(\theta)^\gamma,$$

with parameters σ_0 and γ .

Now, assuming a general power law relationship between σ and θ as:

$$\sigma(\theta) = \beta \theta^\kappa, \quad (16)$$

234 and using (15), the density of PSUs is expressed as:

$$235 \quad N(\theta) = \left(\frac{\sigma_0}{\beta} \right)^{1/\gamma} \theta^{1-\kappa/\gamma}, \quad (17)$$

236 and similarly the average size of a PSU is given by:

$$237 \quad \Gamma(\theta) = \left(\frac{\beta}{\sigma_0} \right)^{1/\gamma} \theta^{\kappa/\gamma}. \quad (18)$$

238 Besides simplicity, expressions of $\sigma(\theta)$, $N(\theta)$ and $\Gamma(\theta)$ in the form of power laws are also
 239 plausible from a biophysical standpoint. It is indeed expected that $\sigma(\theta)$ should be a mono-
 240 tonically increasing function of θ , due to a higher probability of photons absorption. In
 241 contrast, the expressions of $N(\theta)$ and $\Gamma(\theta)$ remain flexible enough with respect to θ , and
 242 so the resulting acclimation model is capable of discrimination between the s-strategy and
 243 n-strategy of PSU acclimation.

244 We note that Camacho and coworkers [14] have used a similar modeling approach and
 245 proposed a monotonically increasing relation between the chlorophyll content θ and the
 246 density of PSUs $N(\theta)$ (which are both decreasing functions of the growth irradiance I_g).
 247 Our model is more flexible in the sense that it enables strategies whereby the chlorophyll
 248 content increases while the density of PSUs decreases.

249 Substituting the power law (16) in the expression of I^* in (13), and log-linearizing the
 250 resulting expression gives:

$$251 \quad \log I^*(\theta) = -\kappa \log \theta - \log(\beta \sqrt{K\tau}). \quad (19)$$

252 The following property follows directly from (19):

253 **Property 2.** *The exponent κ in the power laws (16) corresponds to the (negative) slope in*
 254 *a log-log plot of I^* versus θ .*

255 Like Property 1, the linearity of the relationship between $\log I^*$ and $\log \theta$ can be readily
 256 tested using data from experimental PI curves corresponding to different acclimation states.

257

To summarize, a complete expression of the model predicting the PI responses of a given microalgae at various pre-acclimated states is:

$$\mu_{\text{chl}}^{\text{PI}}(q, \theta, I) = \bar{\alpha} \left(1 - \frac{Q_0}{Q_{\text{max}}(\cdot)} \right) \frac{I}{1 + \tau \beta \theta^{\kappa} I + K \tau \beta^2 \theta^{2\kappa} I^2}. \quad (20)$$

This expression is of the Haldane type with respect to the light intensity I , and it comprises the following parameters: K and τ from the Han model; β and κ from the acclimation model; and the initial slope $\bar{\alpha}$ together with the minimal and maximal nitrogen quotas Q_0 and Q_{max} —or alternatively α in its simplified version.

4. Calibration and Confidence Analysis using Data Sets from the Literature

A calibration of the new features in the coupled model is carried out in this section, using experimental data sets from the works of Anning et al. [1] and Falkowski and Owens [11]. The focus is on the chlorophyll-specific photosynthesis rate (20), the density and size acclimation laws (17)-(18), and the saturation function ψ in the nitrogen-quota-to-chlorophyll-quota relationship (5).

4.1. Data for *Skeletonema costatum*

Experimental data by Anning et al. [1] are for the diatom *Skeletonema costatum*. They comprise two acclimation states at different growth irradiances I_{g} , namely $50 \mu\text{E m}^{-2} \text{s}^{-1}$ (LL) and $1500 \mu\text{E m}^{-2} \text{s}^{-1}$ (HL). The LL irradiance corresponds to a chlorophyll quota of $\theta = 0.082 \text{ g}_{\text{chl}} \text{g}_{\text{C}}^{-1}$, and the HL irradiance to $\theta = 0.018 \text{ g}_{\text{chl}} \text{g}_{\text{C}}^{-1}$. Measurements of the number and size of PSUs are also available for four acclimation states in Falkowski and Owens [11]. Only the number of photosystems I (PSI) is reported and we assume the number of PSUs to be proportional here.

Calibration of PI-Response Curves. We neglect variations of the term α in (20) as a first approximation, and we consider a nonlinear regression approach based on least-square minimization to estimate the values of parameters β , κ and α . On the other hand, we use default values for the Han model parameters k_r , k_d and τ ; these values are obtained by averaging over the parameter ranges reported in [18] and can be found in Table I.

Table I: Default parameter values in the Han model and parameter estimates in the photosynthesis rate (20) for *S. costatum*.

Param.	Value	Source
τ	5.50×10^{-3} [s]	Ref. [18]
k_r	1.40×10^{-4} [s $^{-1}$]	Ref. [18]
k_d	5.00×10^{-6} [-]	Ref. [18]
α	1.60×10^{-2} [g _C g _{chl} $^{-1}$ μ E $^{-1}$ m ²]	estimated
β	4.92×10^{-1} [μ E $^{-1}$ m ² g _{chl} $^{1/\kappa}$ g _C $^{-1/\kappa}$]	estimated
κ	4.69×10^{-1} [-]	estimated

In order to certify global optimality of the parameter estimates, we use the global optimization solver BARON [33] in the GAMS modeling environment. The resulting parameter estimates are given in Table I, and the fitted PI-response curves (20) are plotted against the available experimental data in Fig. 1. The predictions are in excellent agreement with this experimental data sets at both light irradiances, also with regards to Property 1, thereby providing a first validation of the structural assumptions in (20).

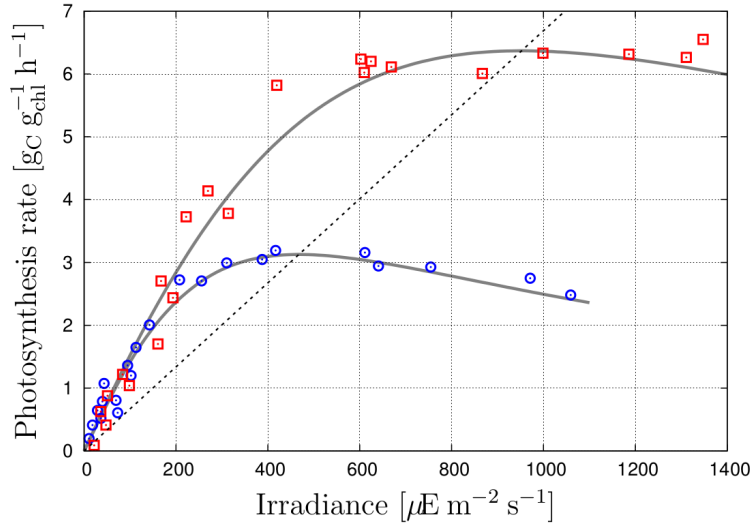


Figure 1: PI-response curves for *S. costatum* based on the data by Anning et al. [1]. The blue and red points correspond to acclimation at LL and HL, respectively. The predicted PI responses are depicted in gray solid lines. The dashed line connects the maxima of both PI curves per Property 1.

In order to assess the confidence of the parameter estimates in Table I, we apply set-membership parameter estimation in the bounded-error sense [21]. To conduct the analysis, we consider variations around the available photosynthesis rate measurements, here vari-

ations of $\pm 5\%$. A large number of scenarios is generated by sampling the resulting measurement ranges—using Sobol sequences and assuming no correlation between the different measurements—and globally optimal estimates for β , κ and α are then computed for every scenario. This way, we obtain the set of all possible parameter values that are consistent with the available measurements within a $\pm 5\%$ error.

The results obtained for the data set by Anning et al. [1] are shown in Fig. 2. Projections of the confidence region onto the (β, κ) , (β, α) and (κ, α) subspaces provide parameter confidence ranges as $\beta \in [0.45, 0.54]$, $\kappa \in [0.44, 0.5]$ and $\alpha \in [0.0158, 0.0172]$. Moreover, these projections reveal the existence of a significant correlation between the parameters β and κ of the acclimation model, whereas correlations of β or κ with α are rather small. The envelopes of both PI-response curves obtained for parameter values in the confidence region are shown on the bottom-right plot of Fig. 2 as well, confirming the good agreement with the experimental data.

Calibration of Density and Size Acclimation Laws. Since experimental information is available for both the density and size of PSUs at four different acclimation states, values of the acclimation parameters σ_0 and κ in the power laws (17)-(18) can be estimated for this data set too. Note that these relationships can be rewritten in the form

$$\begin{aligned} 1/\gamma \log \left(\frac{\sigma_0}{\beta} \right) - \kappa/\gamma \log \theta &= \log N - \log \theta, \\ 1/\gamma \log \left(\frac{\sigma_0}{\beta} \right) - \kappa/\gamma \log \theta &= -\log \Gamma, \end{aligned}$$

thus making it possible to use a simple linear regression approach for estimating the values of $1/\gamma \log \left(\frac{\sigma_0}{\beta} \right)$ and κ/γ . Estimates for the parameters σ_0 and κ , as reported in Table II, can be obtained in turn by using the estimates for β , κ and α in Table I.

Table II: Parameter estimates in the density and size acclimation laws (17)-(18) for *S. costatum*.

Parameter	Value
σ_0	$1.63 \times 10^{-1} [\mu E^{-1} m^2 g_{chl}^{-\gamma} PSU^\gamma]$
γ	$1.18 \times 10^{-1} [-]$

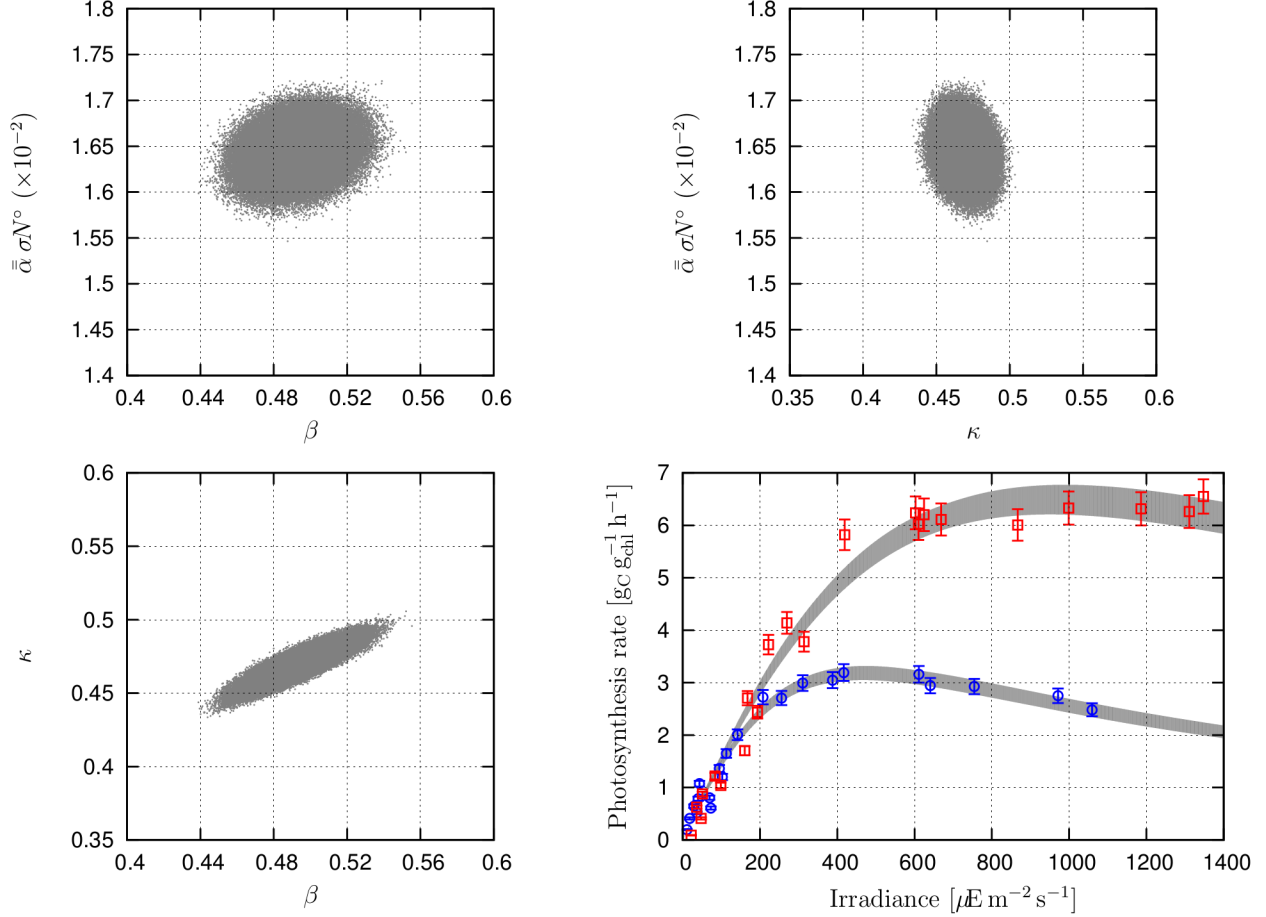


Figure 2: Confidence region of the parameter estimates β , κ and α with $\pm 5\%$ deviations and corresponding envelopes of PI curves for *S. costatum*.

Following a set-membership estimation approach, confidence in the foregoing parameter estimates is assessed by computing the set of all values for σ_0 and κ that are consistent with the available measurement of density and size of PSU (within variations of $\pm 5\%$), while simultaneously accounting for the uncertainty in the values of β , κ and α (Fig. 2). The resulting confidence region is shown on the left plot in Fig. 3, and the set of corresponding model fits for the experimental data on the right plot. Parameter confidence ranges are obtained as $\sigma_0 \in [0.12, 0.51]$ and $\gamma \in [0.08, 0.39]$. Despite being quite conservative, these bounds allow to confidently conclude that the parameter γ is indeed positive for *S. costatum*. This finding will be discussed further in Sect. 5.

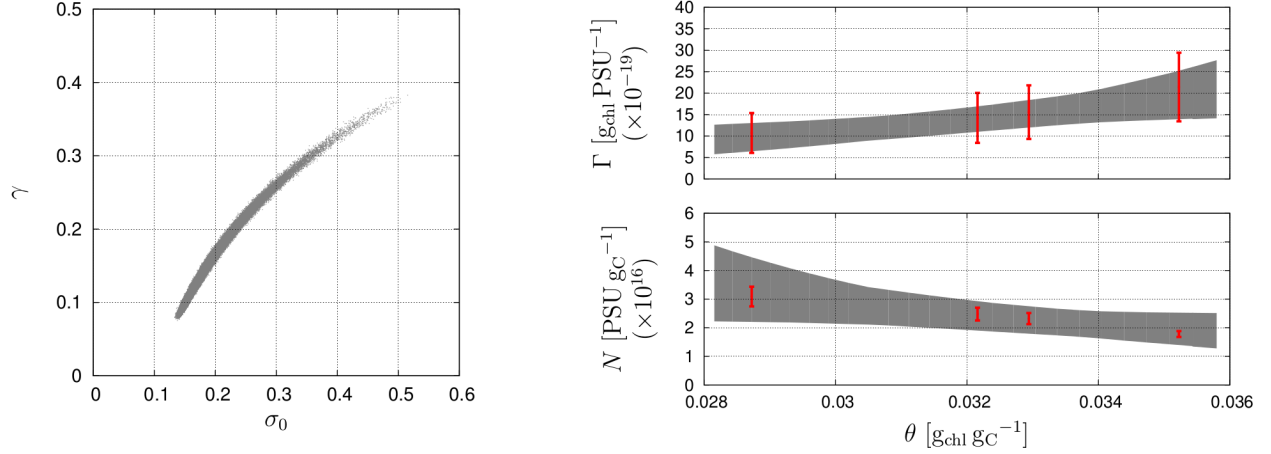


Figure 3: Confidence region of the parameter estimates γ and σ_0 for the measurement data ranges of PSU size and number (left plot) and corresponding fit envelopes (right plots) for *S. costatum*.

4.2. Data for *Dunaliella tertiolecta*

Experimental data by Falkowski and Owens [11] are for the chlorophyte *Dunaliella tertiolecta*. Amongst the available data, four PI curves are selected that were not affected by ‘bleaching’, corresponding to acclimation states at growth irradiances I_g of $60 \mu\text{E m}^{-2} \text{s}^{-1}$ (L_1), $120 \mu\text{E m}^{-2} \text{s}^{-1}$ (L_2), $200 \mu\text{E m}^{-2} \text{s}^{-1}$ (L_3), and $400 \mu\text{E m}^{-2} \text{s}^{-1}$ (L_4). Measurements of carbon, nitrogen and chlorophyll content per cell for all four acclimation states make it possible to determine lower and upper ranges for both the nitrogen quota q and the chlorophyll quota θ as well, as given in Table III. Moreover, measurements of the number and size of PSUs are also available at four acclimation states, assuming that the number of PSUs is proportional to the measured number of PSIs.

Table III: Ranges of nitrogen and chlorophyll quotas from the experimental data by Falkowski and Owens [11] at acclimation states L_1 , L_2 , L_3 and L_4 .

Growth irradiance I_g [$\mu\text{E m}^{-2} \text{s}^{-1}$]	Nitrogen quota Q_{\max} [$\text{g}_\text{N g}_\text{C}^{-1}$]	Chlorophyll quota θ [$\text{g}_\text{chl g}_\text{C}^{-1}$]
L_1 : 60	$Q_{\max} \in [0.250, 0.357]$	$\theta \in [0.0774, 0.0820]$
L_2 : 120	$Q_{\max} \in [0.222, 0.323]$	$\theta \in [0.0654, 0.0682]$
L_3 : 200	$Q_{\max} \in [0.213, 0.286]$	$\theta \in [0.0436, 0.0453]$
L_4 : 400	$Q_{\max} \in [0.172, 0.208]$	$\theta \in [0.0355, 0.0373]$

Calibration of PI-Response Curves. Since experimental information is available for the nitrogen quota q in all acclimation states, variations of the term $(1 - Q_0/Q_{\max})$ in (20) can be accounted for with this data set—we consider a value of $Q_0 = 0.05 \text{ g}_N \text{ g}_C^{-1}$ for the minimal nitrogen quota throughout [16, 2]. Like previously, we use a nonlinear regression approach based on least-square minimization to estimate the values of parameters $\bar{\alpha}$, β and κ , and we define extra variables for the nitrogen and chlorophyll quotas in the regression problem with bounds as defined in Table III. As far as the Han model parameters are concerned, we use the default values of τ and k_r in Table I. On the other hand, the default value for k_d is not deemed suitable as photoinhibition effects are not observed on the available PI-curve data, so k_d is considered an extra variable in the regression problem with bounds $[0, 10^{-7}]$ initially. More data at higher light irradiance would be needed for a better calibration.

Table IV: Parameter estimates in the photosynthesis rate (20) for *D. tertiolecta*.

Param.	Value	Nitrogen quota	Chlorophyll quota
$\bar{\alpha}$	$5.50 \times 10^{-2} \text{ g}_C \text{ g}_{\text{chl}}^{-1} \mu\text{E}^{-1} \text{ m}^2$	$Q_{\max}^{60} = 0.250 \text{ g}_N \text{ g}_C^{-1}$	$\theta^{60} = 0.082 \text{ g}_{\text{chl}} \text{ g}_C^{-1}$
β	$5.48 \times 10^1 \mu\text{E}^{-1} \text{ m}^2 \text{ g}_{\text{chl}}^{1/\kappa} \text{ g}_C^{-1/\kappa}$	$Q_{\max}^{120} = 0.322 \text{ g}_N \text{ g}_C^{-1}$	$\theta^{120} = 0.065 \text{ g}_{\text{chl}} \text{ g}_C^{-1}$
κ	$1.54 \times 10^0 -$	$Q_{\max}^{200} = 0.266 \text{ g}_N \text{ g}_C^{-1}$	$\theta^{200} = 0.045 \text{ g}_{\text{chl}} \text{ g}_C^{-1}$
k_d	$1.27 \times 10^{-8} -$	$Q_{\max}^{400} = 0.208 \text{ g}_N \text{ g}_C^{-1}$	$\theta^{400} = 0.036 \text{ g}_{\text{chl}} \text{ g}_C^{-1}$

The solver BARON [33] in the GAMS modeling environment is again used to guarantee globally optimal parameter estimates. These estimates are reported in Table IV, and the fitted PI-response curves (20) are plotted against the available experimental data in Fig. 4 in gray solid lines. The predicted responses are generally in good agreement with the experimental data, thereby confirming the ability of the model to capture the photosynthetic activity of *D. tertiolecta*.

For sake of comparison, we also plot in gray dotted lines on Fig. 4 the fitted PI responses without accounting for variations of the term $(1 - \frac{Q_0}{Q_{\max}})$ in (20); that is, the parameter α is estimated in lieu of $\bar{\alpha}$. These fits, although slightly degraded, remain accurate. Moreover, the corresponding parameter estimates, $\beta \approx 32.4$, $\kappa \approx 1.4$, and $\alpha \approx 0.042$, are in good agreement with the values in Table IV as well as with the confidence analysis that follows.

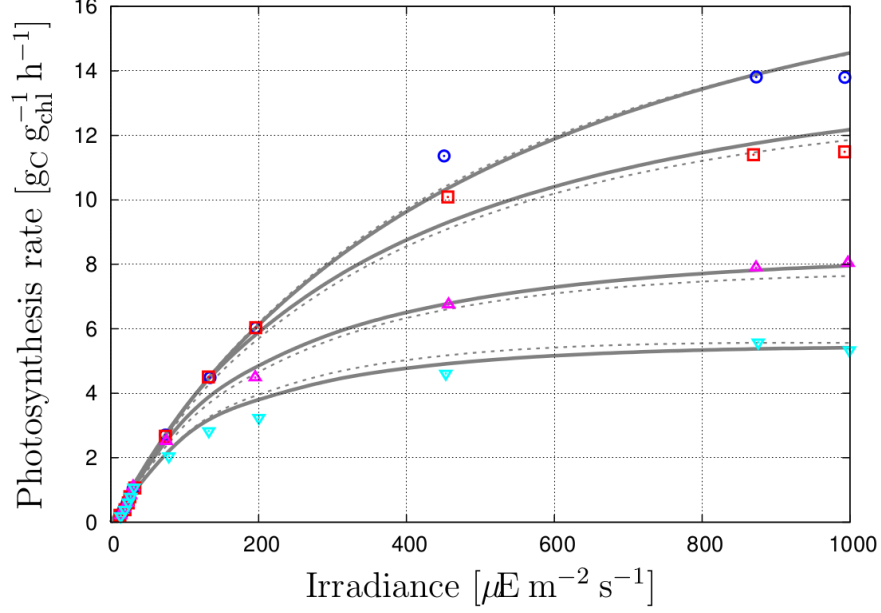


Figure 4: PI-response curves for *D. tertiolecta* based on the data by Falkowski and Owens [11]. The cyan, magenta, red, and blue points correspond to acclimation at L_1 , L_2 , L_3 and L_4 , respectively. The predicted PI responses are depicted in gray lines, with and without accounting for variations of the term $(1 - Q_0/Q_{\max})$ in solid lines and dotted lines, respectively.

This shows that the PI-response model (20) is robust towards uncertainty in the nitrogen maximal quota Q_{\max} .

As previously with *S. costatum*, we assess the confidence of the estimates obtained for the acclimation parameters $\bar{\alpha}$, β and κ in Table IV. We consider variations of $\pm 5\%$ around the available photosynthesis rate measurements and we compute the set of all possible values for $\bar{\alpha}$, β and κ that are consistent with these measurement-error ranges.

The results obtained for the data set by Falkowski and Owens [11] are shown in Fig. 5. Projections of the confidence region onto the (β, κ) , $(\beta, \bar{\alpha})$ and $(\kappa, \bar{\alpha})$ subspaces provide parameter confidence ranges as $\beta \in [32, 65]$, $\kappa \in [1.35, 1.6]$ and $\bar{\alpha} \in [0.052, 0.058]$. These projections also reveal the existence of a strong correlation between the parameters β and κ , which is likely due to the absence of photoinhibition effects in this data set. In contrast, the correlations of β or κ with $\bar{\alpha}$ appear to be rather small. The envelopes of all four PI-response curves obtained for parameter values in the confidence region are shown on the bottom-right plot of Fig. 2, confirming a good agreement with the experimental data.

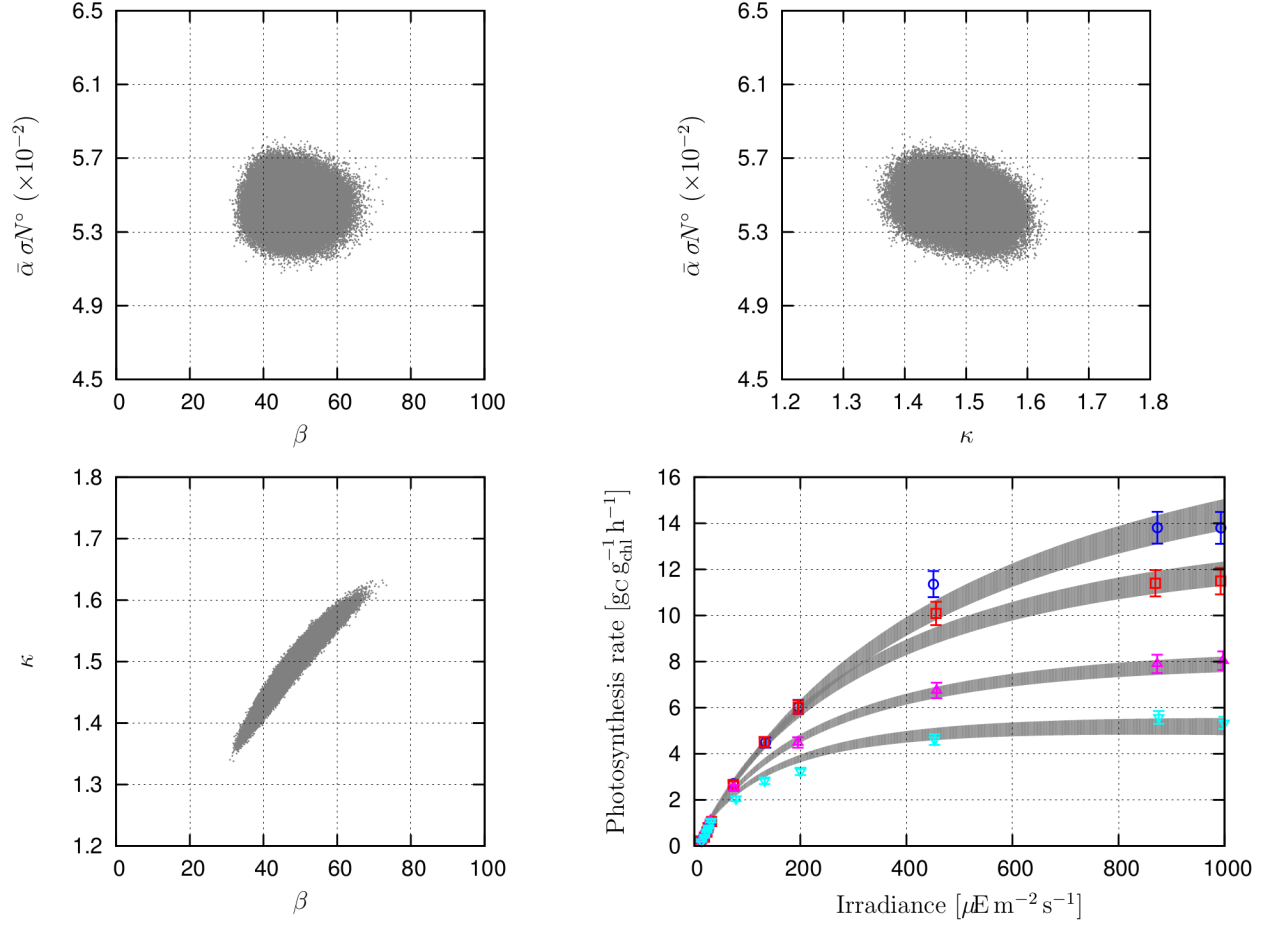


Figure 5: Confidence region of the parameter estimates $\bar{\alpha}$, β and κ with $\pm 5\%$ deviations and corresponding envelopes of PI curves for *D. tertiolecta*.

Calibration of Density and Size Acclimation Laws. Since experimental information is available for both the density and size of PSUs at all four acclimation states, values of the acclimation parameters σ_0 and κ in the power laws (17)-(18) can be estimated for this data set too. We apply the same linear regression approach and confidence analysis as for *S. costatum* in Sect. 4.1. The estimates for the parameters σ_0 and κ in Table II are obtained by using the estimates for β , κ and α in Table IV. Then, confidence in these estimates is assessed by computing the set of all values for σ_0 and κ that are consistent with the available measurement of density and size of PSU (within variations of $\pm 5\%$), while simultaneously accounting for the uncertainty in the values of β , κ and α (Fig. 5).

The resulting confidence region is shown on the left plot in Fig. 6, and the set of corre-

sponding model fits for the experimental data on the right plot. Here, parameter confidence ranges are obtained as $\sigma_0 \in [0, \infty)$ and $\gamma \in (-\infty, -3.5]$. Clearly, the parameter σ_0 is not identifiable for this data, which is due to the fact that the size of PSU remains about constant at various acclimation states, and the range for γ is unbounded from below. Nonetheless, the upper bound for γ still allows to confidently conclude that this parameter is indeed negative for *D. tertiolecta*; see Sect. 5 for further discussion.

Table V: Parameter estimates in the density and size acclimation laws (17)-(18) for *D. tertiolecta*.

Parameter	Value
σ_0	$2.60 \times 10^{-11} [\mu E^{-1} m^2 g_{chl}^{-\gamma} PSU^\gamma]$
γ	$-4.64 \times 10^0 [-]$

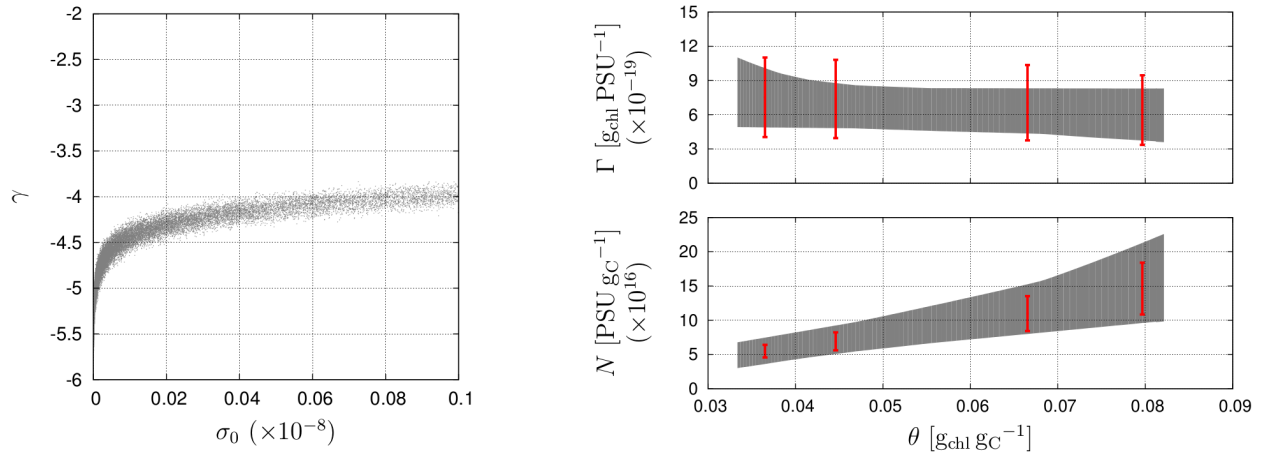


Figure 6: Confidence region of the parameter estimates γ and σ_0 for the measurement data ranges of PSU size and number (left plot) and corresponding fit envelopes (right plots) for *D. tertiolecta*.

Calibration of Nitrogen-Quota-to-Chlorophyll-Quota Relationship. Since experimental information is available for both the nitrogen quota q and the chlorophyll quota θ in all four acclimation states, values of the parameters $\bar{\psi}$ and k_I in the nitrogen-quota-to-chlorophyll-quota relationship (5)-(6) can be estimated from this data set as well. We apply a similar linear regression approach and confidence analysis as for the density and size acclimation

law, noting that the relationships (5)-(6) can be rewritten in the form:

$$\bar{\psi} \frac{q}{\theta} - \frac{1}{k_I} I_g = 1.$$

thus giving estimates for $\bar{\psi}$ and $\frac{1}{k_I}$, as reported in Table VI. For consistency with the previous PI-curve calibration, we use the estimated values of nitrogen and chlorophyll quotas in Table III to carry out the estimation. The nitrogen-quota-to-chlorophyll-quota predictions (black points) are plotted against the available experimental data (red circles) in Fig. 7; the gray dotted line on this plot is merely an interpolation between the predictions, since nitrogen or chlorophyll quotas are not available at intermediate irradiances. Despite some discrepancies at higher light irradiances, these results confirm the ability of the acclimation model (5)-(6) to capture the general trend of the data.

Table VI: Parameter estimates in the nitrogen-quota-to-chlorophyll-quota relationship (5)-(6) for *D. tertiolecta*.

Parameter	Value
$\bar{\psi}$	$0.31 \text{ g}_{\text{chl}} \text{ g}_{\text{N}}^{-1}$
k_I	$440 \text{ } \mu\text{E m}^{-2} \text{ s}^{-1}$

Finally, confidence in the foregoing parameter estimates is assessed by computing the set of all values for $\bar{\psi}$ and k_I that are consistent with the available measurement ranges of the nitrogen quota q and of the chlorophyll quota θ in all four acclimation states. The resulting confidence region is shown on the left plot in Fig. 8, providing parameter confidence ranges as $\bar{\psi} \in [0.2, 0.35]$ and $k_I \in [400, \infty)$. The bounds on $\bar{\psi}$, although wide, confirm the order of magnitude for this parameter. On the other hand, k_I can take on arbitrary large values, a result which is best understood from the upper-right plot in Fig. 8, where a horizontal line can indeed be seen to provide a good fit of the data point due to the large uncertainty in the nitrogen-quota measurements. This uncertainty is also reflected in the rather loose model-prediction envelopes on the lower-right plot.

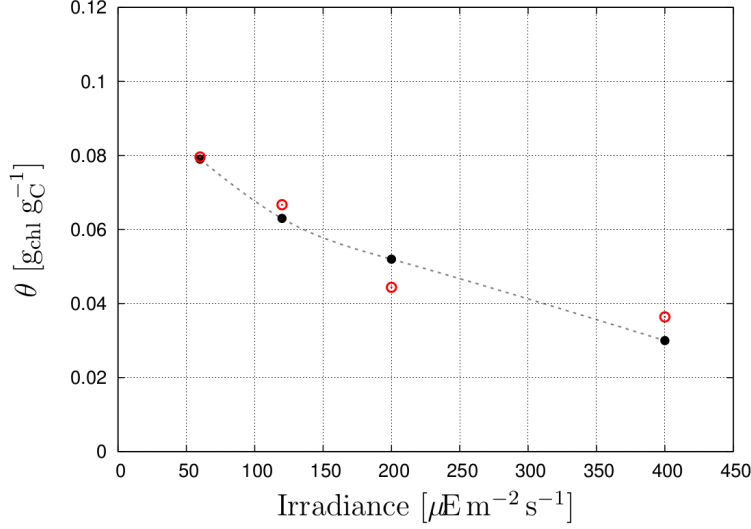


Figure 7: Relation between chlorophyll quota and growth irradiance for *D. tertiolecta*. The red circles correspond to measurements by Falkowski and Owens [11] at acclimation states L_1 , L_2 , L_3 and L_4 , respectively. The black points are computed from the calibrated nitrogen-quota-to-chlorophyll-quota relationship (5)-(6), interpolated by the gray dotted line.

5. Discussion

5.1. Model Extensions and Simplifications

The proposed model in Sect. 3 assumes that only the effective cross-section σ in the Han model is affected by the photoacclimation processes. However, other parameters are likely to vary in response to a change in θ . In particular, there is strong experimental evidence supporting a variation of the parameter τ with the growth irradiance [26, 31]. A more complex model encompassing adaptation of this parameter at the slow time-scale could be considered, for instance by making τ a function of θ . As well as increasing complexity, this extension would nonetheless introduce extra parameters, while the data available for calibration are still scarce. Closer inspection of the model reveals that σ and τ always appear together in (12), in the product terms $\sigma\tau$ and $\sigma\tau^2$ (the latter being more important for describing photoinhibition). It is therefore likely that our modeling of σ with respect to τ indirectly accounts for the variation of τ , and that the estimated parameter is effectively $\sigma\tau$. This hypothesis could however reach its limit in case of strong photoinhibition, as the term $\sigma\tau^2$ may become the dominant one.

It is also important to note that photoacclimation acts at different levels in the proposed

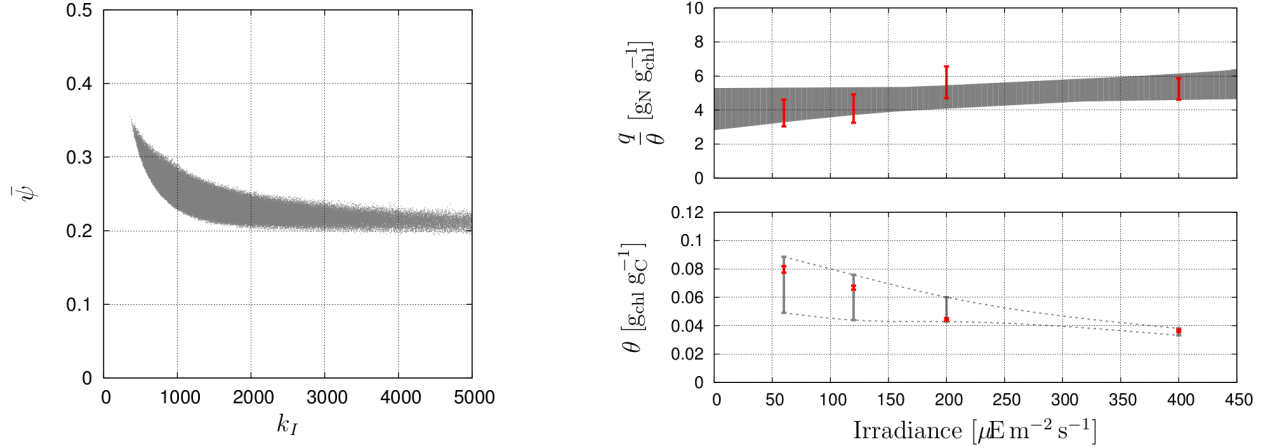


Figure 8: Confidence region of the parameter estimates $\bar{\psi}$ and k_I for the measurement data ranges of nitrogen and chlorophyll quotas given in Table III (left plot) and corresponding fit envelopes (right plots) for *D. tertiolecta*.

model. Direct effect of photoacclimation on growth is via the light-dependent term ϕ in (2), multiplying Droop's classical growth rate. In doing so, we preserve the structure of the Droop model and our model inherits many of its properties. However, both terms ϕ and $(1 - Q_0/q)$ in (2) are increasing functions of the nitrogen quota. It is therefore likely that a simpler model, whereby the term $(1 - Q_0/q)$ is replaced by a constant, may also be capable of accurate predictions. Such a model would in fact be close to the model in [13], which provides a rather simple description of photosynthesis. It is the authors' opinion however that a more structured model as the one in Sect. 3 is preferable given the amount of mathematical analysis that has been devoted to the Droop model over the past few decades.

5.2. Accurate Description of Acclimation Strategies and Parameters

The fits obtained by estimating the parameters β , κ and $\bar{\alpha}$ (or α) in the chlorophyll-specific photosynthesis rate (20) are in good agreement with the two data sets by Anning et al. [1] (Fig. 1) and Falkowski and Owens [11] (Fig. 4). Moreover, the resulting parameter estimates are found to be rather reliable in view of the confidence regions (Figs. 2 and 5), despite the presence of a significant correlation between the acclimation parameters β and κ . For both data sets, information relative to the density and size of PSUs is also available, which allows estimation of the parameters γ and σ_0 as well. Here, the confidence analysis (Figs. 3 and 6) has revealed that σ_0 may turn out to be unidentifiable when the density of

PSU is mainly unaffected by the chlorophyll quota, yet the range of γ can be more reliably estimated. This provides a means of cross-checking the main acclimation mechanism at play, namely the n-strategy versus the s-strategy:

- For *S. costatum* [1], the estimated value and confidence range of κ suggest that the effective cross-section σ is an increasing function of θ per (16), although the rate of increase σ' is slowing down with θ (concave shape); σ is therefore also a decreasing function of the acclimation light I_g . Because of the low small, positive γ value, the average size of PSU is fast increasing with θ , while the density of PSU is fast decreasing. This behavior can thus be interpreted as a mixed n-s acclimation strategy, with predominance of the s-type acclimation, in agreement with Falkowski and Owens [11]. Also worth noting is the fact that the effective cross-section decreases much less rapidly with the acclimation light than the average PSU size, suggesting a reduced packaging effect, possibly due to the relatively small size of this species [24].
- For *D. tertiolecta* [11], the estimated value and confidence range of κ suggest that σ is increasing with θ , but the rate of increase σ' is itself increasing (convex). The average size of PSU remains about constant with θ , while the density of PSU is fast increasing with θ —or, equivalently, fast decreasing with the acclimation light I_g . According to this analysis *D. tertiolecta* would preferentially follow the n-strategy, which is in agreement with [11]. The fact that the effective cross-section is fast decreasing with the acclimation light, while the average size of PSU is about constant, suggests a strategy combining packaging effect and synthesis of accessory pigments in order to protect the cells from high irradiance [30].

In sum, the model represents these two different behaviors, illustrating well its potential to distinguish between competing acclimation strategies for their light harvesting capacity at various irradiance levels. The fundamental differences between such strategies can in fact be related to the ecological niches occupied by both species [11]: *D. tertiolecta* is primarily found in shallow waters at low latitudes, and must therefore deal with high light. *S. costatum* lives in deeper, cooler waters and has to deal with low light intensity.

Regarding the photoacclimation kinetics, the fits obtained by estimating the parameters $\bar{\psi}$ and k_I in the nitrogen-quota-to-chlorophyll-quota relationship (5)-(6) show a good agreement with the data sets by Falkowski and Owens [11] (Fig. 7). It is worth mentioning here that the estimated values of k_I and $\bar{\psi}$ (Table IV) are consistent with those reported in previous work [e.g., 2]. Nonetheless, a more careful confidence analysis (Fig. 8) reveals that the nitrogen-quota measurements carry too much uncertainty to determine reliable estimates, especially for the parameter k_I whose confidence range happens to be unbounded. These calibration results, although promising, clearly delineate the need for more accurate and richer data sets in order to fully validate the proposed model.

5.3. Can the Dynamic Model Predict the Data of Neidhardt et al. [25]?

In this subsection, we consider another set of experimental data from Neidhardt et al. [25] for the microalgae *Dunaliella salina*. They comprise two acclimation states at different growth irradiances of $50 \mu\text{E m}^{-2} \text{s}^{-1}$ (LL) and $2000\text{--}2500 \mu\text{E m}^{-2} \text{s}^{-1}$ (HL). Estimation of primary production is via the O_2 production rate by exposing the pre-acclimated microalgae to a sequence of increasing light irradiances between 4.7 and $4900 \mu\text{E m}^{-2} \text{s}^{-1}$, during 150 s at each irradiance level. Moreover, neither the nitrogen quotas nor the chlorophyll quotas are reported.

As seen from Fig. 9, the initial slopes of the PI-response curves for cultures pre-acclimated at LL and HL differ greatly, which is in apparent contradiction with the constant initial slope assumption discussed in Sect. 3.2. Also reported on this figure (solid lines) are the results of a preliminary calibration showing that such a variation in initial slope can nonetheless be predicted accurately by the proposed model. More specifically, we simulated the experimental protocol in [25], to more accurately account for the actual repair dynamics. In this context, it is not assumed that a quasi steady state is reached for C . The calibration procedure was carried out on this basis. It is important to do so here, because each stage of the PI-response protocol (150 s) may be too short for the dynamics of PSU inhibition to fully equilibrate, especially for a larger chlorophyll quota (LL pre-acclimated state). The initial slope expression is given by (10), with $A = 1 - C$. When microalgae are acclimated

at a high growth irradiance, A is smaller than one, even at very low light intensities, since a fraction of C is still not fully repaired. The lower slope is thus an index of the fraction of damaged PSU. The simulations on Fig. 9 show that, respecting the exact experimental protocol, this behavior can be reproduced by the model. These results illustrate the capability of the proposed model to describe complex couplings between photoinhibition kinetics and photoacclimation.

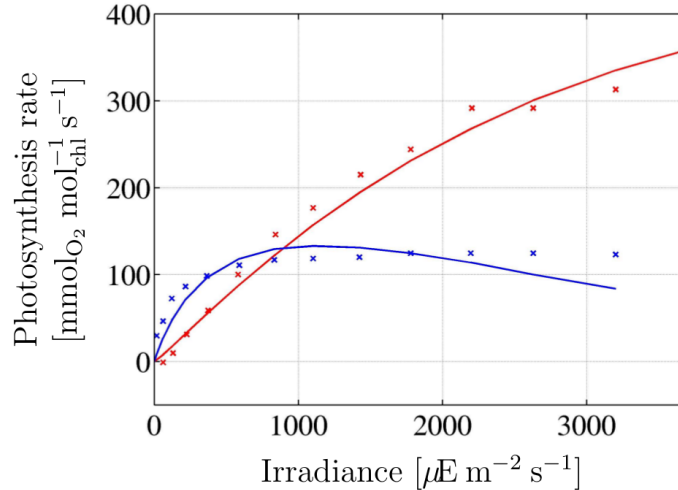


Figure 9: Dependency between growth rate and acclimation for *D. salina* [25]: blue crosses: experimental data for LL acclimation; blue curve: model simulations for LL acclimation; red crosses: experimental data for HL acclimation; red curve: model simulation for HL acclimation.

6. Conclusions and Future Directions

The dynamic model presented in this paper couples photosynthetic processes that act on different time scales. Photosynthetic production and inhibition act on fast time scales of seconds to minutes, while the dynamics of intracellular nitrogen and chlorophyll contents are bound to slow time scales of hours or days. Our model builds upon the well-accepted Droop model describing nitrogen utilization and microalgae growth, together with the Han model describing photoproduction and photoinhibition in terms of PSU states, thereby inheriting their respective properties. The main novelty lies in the use of the chlorophyll quota to relate both the acclimation and growth processes with the states of the PSUs. Combined

with previous (validated) models describing the dynamics of the PSUs (Han model), nitrogen content (Droop model), and chlorophyll content (Geider et al. [15], Bernard [2]), our model is the first of its kind to link photoinhibition, photoacclimation and nutrient-limited growth all together.

Preliminary calibrations and confidence analyses based on PI response data from the literature give encouraging results. By making the link among different PI curves, while preserving a simple structure, the proposed model can serve as a tool for hypothesis testing. Particularly insightful in this context is the ability to distinguish between the s-strategy and the n-strategy of PSU acclimation, which sheds light on the mechanisms that underly photoacclimation in various microalgae species. In order to further discriminate between the n-strategy and s-strategy, more experimental data would be needed nonetheless, especially data covering a wider range of acclimation states and other species. Measuring a larger set of physiological variables, such as the effective cross-section [20], would also be helpful. Another valuable insight from the proposed model has been that the experimental protocols used for producing PI response curves may not allow enough time at each irradiance level for the photoinhibition dynamics to fully develop. In practice, this may lead to overestimating the actual rate of photosynthesis and could explain the variations in initial slopes that are observed between PI response curves at different acclimation states in some experimental studies. Finally, a mathematical analysis of the proposed model could provide valuable insight into the inherent trade-offs and eventually help to identify strategies for enhancing microalgae productivity in large-scale industrial systems.

Acknowledgments

This work was supported by the ANR-13-BIME-0004 Purple Sun together with the INRIA Project Lab Algae in silico. AN and BC gratefully acknowledge financial support from Marie Curie under grant PCIG09-GA-2011-293953.

References

- [1] Anning, T., MacIntyre, H. L., Pratt, S. M., Sammes, P. J., Gibb, S. and, R. J., 2000. Photoacclimation in the marine diatom *Skeletonema costatum*. Limnology & Oceanog-

raphy 45, 1807–1817.

- [2] Bernard, O., 2011. Hurdles and challenges for modelling and control of microalgae for CO₂ mitigation and biofuel production. *Journal of Process Control* 21 (10), 1378–1389.
- [3] Bernard, O., Gouzé, J. L., 1995. Transient behavior of biological loop models, with application to the Droop model. *Mathematical Biosciences* 127 (1), 19–43.
- [4] Bernard, O., Gouzé, J. L., 1999. Nonlinear qualitative signal processing for biological systems: application to the algal growth in bioreactors. *Mathematical Biosciences* 157, 357–372.
- [5] Bernard, O., Mairet, F., Chachuat, B., 2015. Modelling of microalgae culture systems with applications to control and optimization. In: Posten, C., (Ed), *Microalgae Biotechnology. Advances in Biochemical Engineering/Biotechnology*, in press (DOI: 10.1007/10_2014_287).
- [6] Brennan, L., Owende, P., 2010. Biofuels from microalgae: a review of technologies for production, processing, and extractions of biofuels and co-products. *Renewable & Sustainable Energy Reviews* 14 (2), 557 – 577.
- [7] Droop, M. R., 1968. Vitamin B₁₂ and marine ecology. The kinetics of uptake, growth and inhibition in *Monochrysis lutheri*. *Journal of the Marine Biological Association of the United Kingdom* 48 (3), 689–733.
- [8] Droop, M. R., 1983. 25 years of algal growth kinetics – A personal view. *Botanica Marina* 16, 99–112.
- [9] Eilers, P., Peeters, J., 1993. Dynamic behaviour of a model for photosynthesis and photoinhibition. *Ecological Modelling* 69 (1-2), 113–133.
- [10] Eilers, P. H. C., Peeters, J. C. H., 1993. Dynamic behavior of a model for photosynthesis and photoinhibition. *Ecological Modelling* 69 (1-2), 113–133.
- [11] Falkowski, P. G., Owens, T. G., 1980. Light-shade adaptation: Two strategies in marine phytoplankton. *Plant Physiology* 66, 592–595.
- [12] Falkowski, P. G., Raven, J. A., 2007. *Aquatic Photosynthesis*, 2nd Edition. Princeton University Press.
- [13] Faugeras, B., Bernard, O., Sciandra, A., Levy, M., 2004. A mechanistic modelling and data assimilation approach to estimate the carbon/chlorophyll and carbon/nitrogen ratios in a coupled hydrodynamical-biological model. *Nonlinear Processes in Geophysics* 11, 515–533.
- [14] Garcia-Camacho, F., Sanchez-Miron, A., Molina-Grima, E., Camacho-Rubio, F., Merchuck, J. C., 2012. A mechanistic model of photosynthesis in microalgae including photoacclimation dynamics. *Journal of Theoretical Biology* 304, 1–15.

- [15] Geider, R. J., MacIntyre, H. L., Kana, T. M., 1997. Dynamic model of phytoplankton growth and acclimation: responses of the balanced growth rate and the chlorophyll *a*:carbon ratio to light, nutrient-limitation and temperature. *Marine Ecology Progress Series* 148, 187–200.
- [16] Geider, R. J., MacIntyre, H. L., Kana, T. M., 1998. A dynamic regulatory model of phytoplanktonic acclimation to light, nutrients, and temperature. *Limnology & Oceanography* 43 (4), 679–694.
- [17] Han, B. P., 2001. Photosynthesis-irradiance response at physiological level: A mechanistic model. *Journal of Theoretical Biology* 213, 121–127.
- [18] Han, B. P., Virtanen, M., Koponen, J., Straskraba, M., 2000. Effect of photoinhibition on algal photosynthesis: a dynamic model. *Journal of Plankton Research* 22 (5), 865–885.
- [19] Hartmann, P., Béchet, Q., Bernard, O., 2014. The effect of photosynthesis time scales on microalgae productivity. *Bioprocess & Biosystems Engineering* 37 (1), 17–25.
- [20] Huot, Y., Babin, M., 2010. *Chlorophyll *a* Fluorescence in Aquatic Sciences: Methods and Applications*. Springer, Dordrecht, The Netherlands.
- [21] Jaulin, L., Walter, E., 1993. Set-inversion via interval analysis for nonlinear bounded-error estimation. *Automatica* 29 (4), 1053–1064.
- [22] Lange, K., Oyarzun, F. J., 1992. The attractiveness of the Droop equations. *Mathematical Biosciences* 111, 261–278.
- [23] MacIntyre, H. L., Kana, T. M., , T., Geider, R. J., 2002. Photoacclimation of photosynthesis irradiance response curves and photosynthetic pigments in microalgae and cyanobacteria. *Journal of Phycology* 38 (1), 17–38.
- [24] Morel, A., Bricaud, A., 1981. Theoretical results concerning light absorption in a discrete medium, and application to specific absorption of phytoplankton. *Deep Sea Research Part A. Oceanographic Research Papers* 28 (11), 1375–1393.
- [25] Neidhardt, J., Benemann, J., Zhang, L., Melis, A., 1998. Photosystem-ii repair and chloroplast recovery from irradiance stress: relationship between chronic photoinhibition, light-harvesting chlorophyll antenna size and photosynthetic productivity in *Dunaliella salina* (green algae). *Photosynthesis Research* 56 (2), 175–184.
- [26] Quigg, A., Kevekordes, K., Raven, J. A., Beardall, J., 2006. Limitations on microalgal growth at very low photon fluence rates: the role of energy slippage. *Photosynthesis research* 88 (3), 299–310.
- [27] Richardson, K., Beardall, J., Raven, J., 1983. Adaptation to unicellular algae to irradiance: An analysis of strategies. *New Phytologist* 93, 175–191.

- [28] Sciandra, A., Ramani, P., 1994. The limitations of continuous cultures with low rates of medium renewal per cell. *Journal of Experimental Marine Biology & Ecology* 178, 1–15.
- [29] Sialve, B., Bernet, N., Bernard, O., 2009. Anaerobic digestion of microalgae as a necessary step to make microalgal biodiesel sustainable. *Biotechnology Advances* 27, 409–416.
- [30] Sosik, H. M., Mitchell, B. G., 1981. Absorption, fluorescence, and quantum yield for growth in nitrogen-limited *Dunaliella tertiolecta*. *Limnology & Oceanography* 36 (5), 910–921.
- [31] Sukenik, A., Bennett, J., Falkowski, P. G., 1987. Light-saturated photosynthesis – limitation by electron transport or carbon fixation? *Biochimica et Biophysica Acta (BBA)-Bioenergetics* 891 (3), 205–215.
- [32] Talec, A., Philistin, M., Ferey, F., Walenta, G., Irisson, J. O., Bernard, O., Sciandra, A., 2013. Effect of gaseous cement industry effluents on four species of microalgae. *Bioresource Technology* 143, 353–359.
- [33] Tawarmalani, M., Sahinidis, N. V., 2005. A polyhedral branch-and-cut approach to global optimization. *Mathematical Programming* 103 (2), 225–249.
- [34] Vatcheva, I., deJong, H., Bernard, O., Mars, N. J. L., 2006. Experiment selection for the discrimination of semi-quantitative models of dynamical systems. *Artificial Intelligence* 170, 472–506.
- [35] Wijffels, R. H., Barbosa, M. J., 2010. An outlook on microalgal biofuels. *Science* 329 (5993), 796–799.
- [36] Williams, P. J. l. B., Laurens, L. M. L., 2010. Microalgae as biodiesel and biomass feedstocks: Review and analysis of the biochemistry, energetics and economics. *Energy & Environmental Science* 3, 554–590.
- [37] Zonneveld, C., 1997. Modeling effects of photoadaptation on the photosynthesis-irradiance curve. *Journal of Theoretical Biology* 186 (3), 381–388.
- [38] Zonneveld, C., 1998. Photoinhibition as affected by photoacclimation in phytoplankton: A model approach. *Journal of Theoretical Biology* 193 (1), 115–123.

Table VII: List of symbols and acronyms.

Symbol	Description	Units
s	inorganic nitrogen concentration	$g_N m^{-3}$
s_{in}	inorganic nitrogen inlet concentration	$g_N m^{-3}$
x	biomass concentration	$g_C m^{-3}$
c	chlorophyll-a concentration	$g_{chl} m^{-3}$
q	carbon-specific nitrogen quota	$g_N g_C^{-1}$
Q_0	minimal carbon-specific nitrogen quota	$g_N g_C^{-1}$
Q_l	nitrogen uptake limit of carbon-specific nitrogen quota	$g_N g_C^{-1}$
Q_{max}	maximal carbon-specific nitrogen quota	$g_N g_C^{-1}$
ψ	nitrogen-specific chlorophyll quota	$g_{chl} g_N^{-1}$
$\bar{\psi}$	maximal nitrogen-specific chlorophyll quota	$g_{chl} g_N^{-1}$
θ	carbon-specific chlorophyll quota	$g_{chl} g_C^{-1}$
D	dilution rate	s^{-1}
μ	biomass growth rate	s^{-1}
$\bar{\mu}$	biomass growth rate under nutrient-replete conditions	s^{-1}
$\mu_{chl}, \mu_{chl}^{PI}$	chlorophyll-specific photosynthesis rate	$g_C g_{chl}^{-1} s^{-1}$
μ_{chl}^{PI*}	optimal chlorophyll-specific photosynthesis rate	$g_C g_{chl}^{-1} s^{-1}$
R	biomass respiration rate	s^{-1}
ρ	inorganic nitrogen uptake rate	$g_N g_C^{-1} s^{-1}$
$\bar{\rho}$	inorganic nitrogen maximal uptake rate	$g_N g_C^{-1} s^{-1}$
k_s	half-saturation constant for inorganic nitrogen uptake rate	$g_N m^{-3}$
ϕ	light-dependent growth term	—
k_I	saturation parameter of the nitrogen-specific chlorophyll-a quota	$\mu E m^{-2} s^{-1}$
I_g	growth irradiance	$\mu E m^{-2} s^{-1}$
I	instantaneous light intensity	$\mu E m^{-2} s^{-1}$
I^*	optimal acclimation irradiance	$\mu E m^{-2} s^{-1}$
δ	photoacclimation time constant	—
A	fraction of photosynthetic units in open state	—
A^∞	steady-state fraction of photosynthetic units in open state	—
B	fraction of photosynthetic units in closed state	—
C	fraction of photosynthetic units in inhibited state	—
σ	effective cross-section of a photosynthetic unit	$m^2 \mu E^{-1}$
τ	turnover time of a photosynthetic unit	s
k_d	damage constant of a photosynthetic unit	—
k_r	repair constant of a photosynthetic unit	s^{-1}
K	ratio of damage to repair constants	s
$\alpha, \bar{\alpha}$	initial slope of the photosynthesis-irradiance response curve	$g_C g_{chl}^{-1} \mu E^{-1} m^2$
Γ	size of a photosynthetic unit	$g_{chl} PSU^{-1}$
N	number of photosynthetic units	$PSU g_C^{-1}$
γ	exponent of photosynthetic unit size equation	—
σ_0	pre-exponential factor of photosynthetic unit size equation	$\mu E^{-1} m^2 g_{chl}^{-\gamma} PSU^\gamma$
κ	exponent of effective cross-section equation	—
β	pre-exponential factor of effective cross-section equation	$\mu E^{-1} m^2 g_{chl}^{1/\kappa} g_C^{-1/\kappa}$
PSI	photosystem I	
PSU	photosynthetic unit	
PI	photosynthesis-irradiance	